Optical techniques for direct imaging of exoplanets/Techniques optiques pour l'imagerie directe des exoplanètes

The Lyot Project: status and results

Anand Sivaramakrishnan [a,*], Ben R. Oppenheimer [a], Sasha Hinkley [a], Douglas Brenner [a], Rémi Soummer [a], Jacob L. Mey [b], James P. Lloyd [c], Marshall D. Perrin [d], James R. Graham [d], Russell B. Makidon [e], Lewis C. Roberts Jr. [f], Jeffrey R. Kuhn [g]

[a] *Astrophysics Department, American Museum of Natural History, 79th Street and Central Park West, New York, NY 10024, USA*
[b] *Microscopy and Imaging Facility, American Museum of Natural History, 79th Street and Central Park West, New York, NY 10024, USA*
[c] *Astronomy Department, Cornell University, 230 Space Sciences Building, Ithaca, NY 14853, USA*
[d] *Astronomy Department, 601 Campbell Hall, University of California, Berkeley, CA 94720, USA*
[e] *Space Telescope Science Institute, 3700 San Martin Drive, Baltimore, MD 21218, USA*
[f] *The Boeing Company, 535 Lipoa Pkwy, Suite 200, Kihei, HI 96753, USA*
[g] *Institute for Astronomy, University of Hawaii, 2680 Woodlawn Drive, Honolulu, HI 96822, USA*

Available online 7 June 2007

Abstract

We present a retrospective on, and some new imaging data from The Lyot Project JHK coronagraph which is used behind the 3.6 m AEOS 941-channel AO telescope on Mt. Haleakala, on the island of Maui in Hawaii. This instrument is the first 'extreme adaptive optics' (ExAO) coronagraph ever; it opens up new scientific search spaces in direct imaging of faint companions of nearby stars. It also blazed a trail for current ExAO systems being developed for ESO-VLT and Gemini telescopes. Amongst other things, the Lyot Project has been used to demonstrate a device for precision coronagraphic astrometry and photometry using the novel technique of placing a wire grid over the pupil to create stable fiducial ghost images, to show the effects of frozen actuators on a deformable mirror, to refine angular differential imaging for use on the Coudé focus of Alt-Az telescopes, and to develop a coronagraphic data reduction pipeline. ***To cite this article: A. Sivaramakrishnan et al., C. R. Physique 8 (2007).***
© 2007 Académie des sciences. Published by Elsevier Masson SAS. All rights reserved.

Résumé

Le projet Lyot : état actuel et résultats. Cet article présente un historique et quelques résulats du coronographe du 'Lyot Project', installé sur le télescope AEOS de 3,6 m à Maui (Hawaii). Cet instrument est le premier coronographe à fonctionner avec une optique adaptive extrême (941 actuateurs) qui ouvre de nouvelles possibilités pour la recherche de compagnons faibles en bande JHK autour d'étoiles proches. Cet instrument est également un précurseur pour les projets en développement comme ESO/SPHERE ou Gemini/GPI. En particulier, il a été utilisé pour tester un dispositif permettant l'astrométrie et la photométrie de précision en mode coronograhique grâce à une grille en plan pupille pour former des images satellites stables de l'étoile. Les données du projet Lyot ont également permis de montrer les effets des actuateurs bloqués sur un miroir déformable, de raffiner la technique d'imagerie différentielle angulaire dans le cas d'observations au foyer coudé d'un télescope Alt-Az et de développer une

* Corresponding author.
  E-mail addresses: anand@amnh.org (A. Sivaramakrishnan), bro@amnh.org (B.R. Oppenheimer), shinkley@amnh.org (S. Hinkley), dbrenner@amnh.org (D. Brenner), rsoummer@amnh.org (R. Soummer), jpl@astro.cornell.edu (J.P. Lloyd), mperrin@astron.berkeley.edu (M.D. Perrin), jrg@astron.berkeley.edu (J.R. Graham), makidon@stsci.edu (R.B. Makidon), Lewis.C.Roberts@zzzz.mil (L.C. Roberts Jr.), kuhn@ifa.hawaii.edu (J.R. Kuhn).

méthode pour le traitement de données coronographiques. ***Pour citer cet article : A. Sivaramakrishnan et al., C. R. Physique 8 (2007).***

1. Introduction

The Lyot Project diffraction-limited near infrared (nIR) stellar coronagraph arose out of the early use of the Palomar 249-channel adaptive optics (AO) system [1] and the diffraction-limited coronagraph in its dedicated PHARO camera [2], combined with theoretical investigations of the way such coronagraphs and AO systems must be matched [3] in order to study the environs of nearby young stars and planet-forming regions. The theory was tested against explorative data taken with the PHARO coronagraph [4]. This exercise demonstrated that high order AO systems were well-suited to Lyot coronagraphy [5] in order to search for faint companions to nearby stars. It also laid out some basic parameters which describe both the Gemini Planet Imager and the ESO VLT SPHERE ExAO systems under development today [6,7].

The Lyot Project coronagraph is deployed behind the 941-actuator AO system on the 3.6 m AEOS telescope on Haleakala on the island of Maui, in Hawaii. Science targets for the instrument are stars brighter than $V = 7$ within 35 pc of the solar system that are accessible from AEOS. This brightness limit is set by AO system wavefront sensor requirements.

Kermit, the camera behind the Lyot Project coronagraph, uses a HAWAII-2 HgCdTe Rockwell detector with several readout modes implemented in its control electronics [8,9]. It also contains a Wollaston prism and liquid crystal variable retarders (LCVRs) to enable a simultaneous dual polarization mode that is now our standard mode of operation.

The coronagraph has been used to study the effects of tip tilt [10] and higher order [11] aberrations, secondary support spiders [12], atmospheric scintillation [13], astrometric and photometric methods, and the effects of immobile actuators on ExAO coronagraphy [14,15]. All these studies break new ground in astronomical imaging. In addition, data reduction methods for dual channel coronagraphic polarimetry were developed. As expected, the data has provided interesting challenges for simple coronagraphic theory and operating concepts

The during the design, construction, and use of the Lyot Project coronagraph several practical issues came to light. We describe these issues and possible solutions for them, some of which we implemented on-sky. While the first few years of operation were severely hampered by bad weather and observatory equipment failures, in this period we achieved several objectives:

 (i) The detection of protoplanetary disks in polarized light in a two minute exposure, indicating the potential of this technique for disk imaging (see also [16]). In comparison, the HST NICMOS' Camera 2 required 120 minutes in order to detect this disk (we defer the discussion of simultaneous dual-channel polarimetry to another paper);
 (ii) Our early data also uncovered a puzzling faint common proper motion companion of an A3V star;
(iii) The development of a basic coronagraphic data reduction pipeline (typical dithering or nodding that is often used in direct imaging is not possible with coronagraphic imaging if the detector is fixed with respect to the focal plane mask (FPM) occulting spot;
(iv) A definition and solution of the problem of high dynamic range astrometry—the position of a faint companion cannot be measured in the same data frame as the bright central object [17]. We devised a solution for this problem by inducing stable ghost images of the primary star, which are used for both astrometric and photometric measurements ([18], see also [19]).

We also plan to field an apodized pupil Lyot coronagraph [20–22] as well as an integral field unit spectrograph in the Lyot Project in the next two years.

The Lyot Project continues to be a stepping stone for next generation Extreme AO (ExAO) systems such as the Gemini Planet Imager [6] and the ESO SPHERE [7] projects, both of which are scheduled for first light in about four years.

2. Optical and mechanical design

2.1. Optical layout

The instrument is described in detail in [23]. We summarize our design here (see Fig. 1). The coronagraph is mounted on a table in a Coudé room. Its electronics and computers are located in an adjoining room. The input beam is $f/200$, with a pupil image 10.4 cm across. This beam is compressed to 10 mm by two nickel-plated, gold-coated off-axis aluminium parabolae manufactured by AXSYS.

At a pupil image past the second off-axis parabola, a flat fast steering mirror (FSM) mounted on a piezo-electrically actuated tip-tilt stage controls the placement of the direct image on the Focal Plane Mask (FPM). In order to form this image light hits a large spherical mirror, coming to a $f/57.25$ focus on the FPM. The FSM is situated 2 cm further along the beam path than the actual pupil image, which permits pupil motion of up to 0.03% of the beam diameter. Electronic control of the FSM has a resolution of 28 microarcseconds on sky, which is well below optical and hardware control tolerances. Science light is reflected off the FPM, but light passing through the hole in the flat mirror falls on a 4-lenslet array that feeds the four fibers that conduct this light to four avalanche photodiodes (APDs) which are read at 2 kHz to provide tip-tilt information. In 0.5 ms a sufficient number of photons can be detected from stars brighter than 4th magnitude in the 0.7 to 1 μm range (the range of sensitivity for the APDs) to provide a centroid with a precision of 57 mas. Fig. 2 shows the 445 μm hole, which, at $f/57.25$, corresponds to 4.71 resolution elements at a wavelength of 1.65 μm. FPM masks with diameters of 245, 334, 445, and 1050 μm were manufactured. The FPM hole imperfections visible at right in Fig. 2 do not appear to limit instrument performance, although a quantitative reconciliation of our FPM knowledge with our best data is still in progress.

After reflecting off the FPM, the IR science light is sent back to the same spherical mirror to produce a Lyot pupil image which is monitored with a CCD camera. I band data from this camera is used in a slow pupil alignment loop by means of an actuated fold mirror. Lyot stops with inner and outer diameters (1.559, 2.541), (1.287, 2.813),
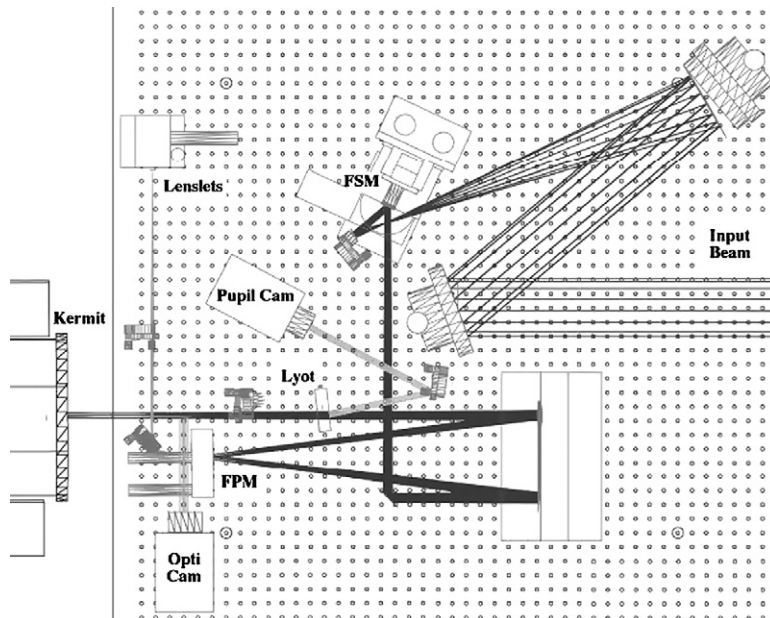

Fig. 1. Layout of the Lyot Project coronagraph showing nIR JHK science light and I band Lyot pupil viewing light paths. The 10.4 cm input beam is compressed by two off-axis parabolae to 10 mm. Kermit is a telecentric camera which contains a YLF Wollaston prism that enables simultaneous dual-channel polarization. See the text for details.
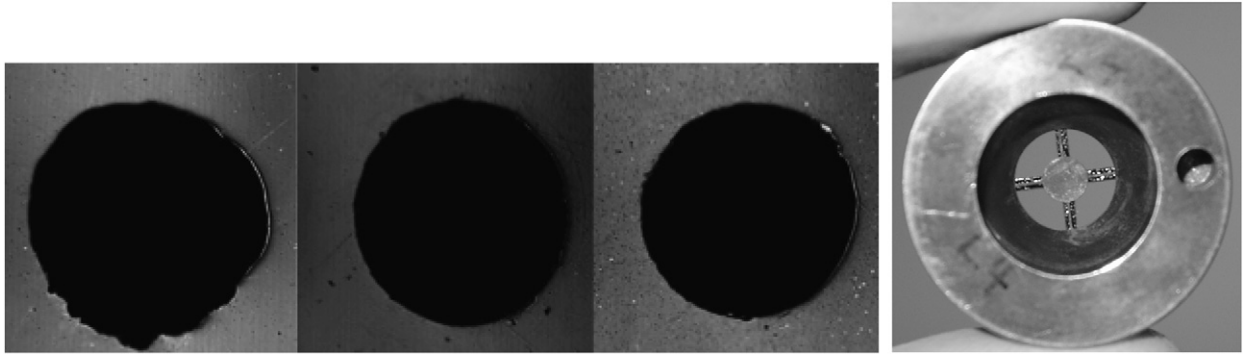
Fig. 2. Left panel: Three micrographs showing stages of FPM hole development. Left: Diamond turned steel with a gold optical coating. Middle: Diamond turned steel with a polished nickel layer coated with gold. Right: Diamond turned nickel polished with a gold coating. This last method was judged to be superior on the basis of these kinds of data, and was used in the instrument. Glass was also tried. The resolution in these images is approximately 0.4 microns. Right panel: Rear surface of a Lyot stop, showing the thickened spider support obstruction. Prior to this modification, coronagraphic images showed strong speckling with the symmetry and morphology of the spiders.

and (0.781, 3.319) meters (as projected back to the primary mirror) are available. These geometries were selected to optimize coronagraphic suppression of the first few Airy rings outside the edge of the FPM, following the prescription described in [3].

The pupil-viewing CCD camera can also collect video-rate data for pupil illumination studies [13,24,15]. During the December 2006 run the spider obstructions in the Lyot stop were widened (Fig. 2). This reduced spider-related noise seen in earlier data, and discussed theoretically by [12]. No instrument-specific numerical studies were performed to support the modification, but it proved highly efficacious nevertheless. In addition, just before the run, the AEOS deformable mirror (DM) was replaced with a fully-functioning DM. A marked improvement in coronagraphic image quality was apparent in images, although this has not been fully quantified yet. Early examination of recent data confirms predictions in [14,15] qualitatively.

2.1.1. Comparison with space-based instruments

In comparison, the HST Advanced Camera for Surveys (ACS) has 1.8 and 3 arcsecond occulters in a beam with half a wave of spherical aberration at V at the mask focus. The Lyot Project coronagraph's field of view is comparable in size to the better (larger) occulting spot of ACS. Thus our search region is complementary to ACS's search space. HST NICMOS' Camera 2 has a rough-edged 0.6 arcsecond diameter occulting hole at a >90% Strehl ratio image, but it lacks an undersized, coronagraphically optimized Lyot stop which would provide optimal coronagraphic suppression. Thus the raw contrast in images is not as good as that obtained by the Lyot Project. However, the relative stability of the HST PSF improves contrast in processed images at wider separations, again, outside the field of view of the Lyot Project coronagraph. HST STIS lacks an optimized Lyot stop in its occulting bar. The primary purpose of the STIS occulter is to reduce demand on the detector when it is illuminated by a bright source, very much like the NICMOS coronagraph. STIS operates in the UV. Thus the Lyot Project coronagraph is complementary to HST instruments.

2.2. Kermit camera detector control

2.2.1. Optics

Kermit is built around a Rockwell HAWAII-2 2048 × 2048 pixel detector (Rockwell Scientific Corporation) as a high dynamic range JHK camera (Fig. 3). It also possesses re-imaging optics that allow for a cold pupil stop within the dewar. It uses a unit magnification, telecentric Offner relay, which consists of two concentric spherical mirrors with radii of curvature related by $R_1 = 2R_2$. Optical design took place at the University of Hawaii Institute for Astronomy (IfA), with fabrication by IR Labs (Tucson, AZ) and the IfA Scientific Instrument Shop. Further details can be found in [9].
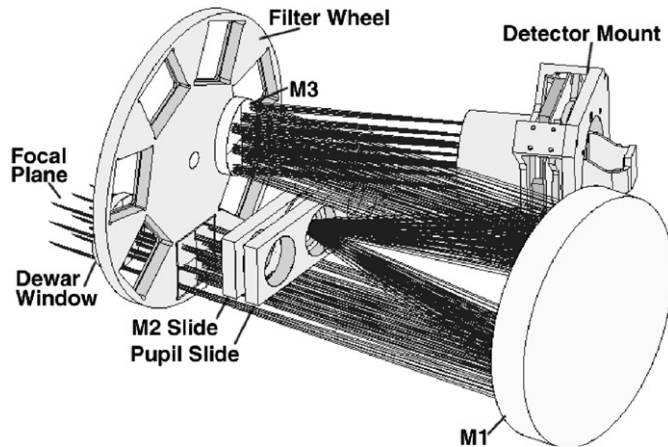
Fig. 3. Optomechanical layout of Kermit.

2.2.2. Electronics and detector readout

Readout electronics and control software for Kermit are based upon the widely used readout electronics system available from Astronomical Research Cameras, Inc., and software developed for the Lick Observatory AO system's IRCAL camera [8].

The detector is sensitive between 0.8 and 2.5 μm, with roughly 60% quantum efficiency across that range. Full well depth is 10^5 electrons, with dark current <0.03 electrons/second at 78 K and read noise <10 electrons using correlated double sampling.

Readout electronics for Kermit is a 32-channel Generation II system supplied by Astronomical Research Cameras (ARC) of San Diego, CA. Our configuration features an ARC Gen II timing board, clock and bias driver board, and eight four-channel A/D converter and coadder boards, along with the standard power regulation board and power supply.

The 32 output channels from the detector are connected directly to two-stage amplifiers on the eight A/D converter boards using low-noise Analog Devices AD829 op-amps, and then digitized by ADS931 16-bit ADCs with a conversion time of 1 μs. The digital output is stored into 32-bit × 1 Megaword RAM buffers directly on the co-adder boards, allowing a maximum readout rate of 32 megapixels/second, or 8 Hz full frame rate. Three layers of control software exist between the camera hardware and the user. The readout electronics are controlled by nine Motorola 56002 digital signal processors (DSPs), one on each A/D board and a master controller on the timing board, which is responsible for producing the readout waveforms. Two readout speeds are supported: 4 μs/pixel and 2 μs/pixel, with the default 4 μs. Using the 4 μs pixel time, it therefore takes 524 ms to clock out a full frame. Faster frame rates are available by reading out only a subarray, down to 16 ms for a 64 × 64 pixel readout.

On the control computer a daemon interfaces with the readout electronics. The third software layer is a graphical TCL/Tk user interface (GUI) which provides a top-level interface for controlling the camera. The camera daemon and GUI communicate via TCP sockets using the Lick Observatory Traffic message passing library.

2.3. Astrometric and photometric grid

Since coronagraphic astrometry is challenging unless special provisions are made to create fiducials [17–19], we used the approach described in detail in [18]. An astrometric grid with 22 152.4 μm-thick wires stretched in two orthogonal directions is located at the 104 mm pupil in the Coudé room. This grid produces four satellite stripes centered 1.97 arcseconds from the occulted star as a positional and photometric fiducial. These stripes are approximately 5 resolution elements (almost 0.2 seconds of arc) long in the 20% fractional bandpass *H* band. The surface brightness of these stripes is about 9.3 magnitudes fainter than the occulted star. The speckle noise limit in single exposures at such angular separations from the central star is about 11 magnitudes [25]. These fiducial stripes can be used to align individual exposures with a high degree of accuracy. Fig. 4 shows such a grid, and data taken using it. The fiducials are clearly visible above speckle noise in this unprocessed data frame. Further work on calibrating these fiducials and
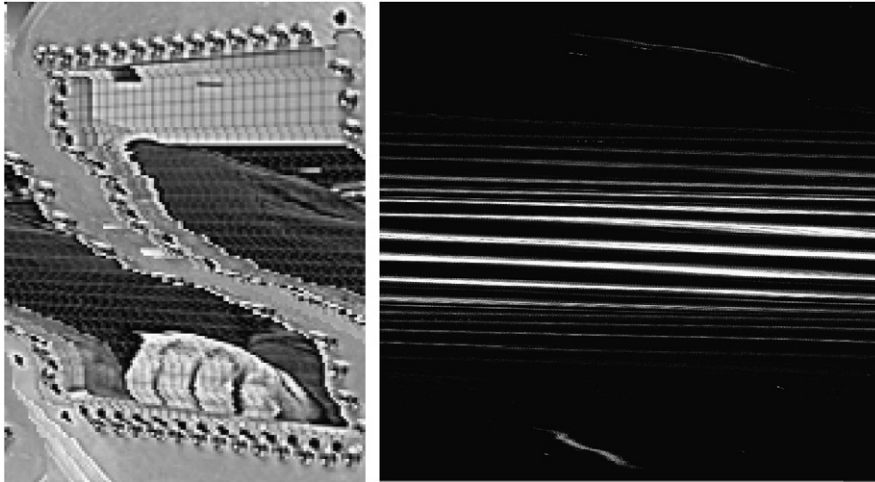
Fig. 4. The astrometric and photometric grid (left) and a coronagraphic H-band image when the grid is placed over the pupil (right). Wires 150.2 μm are wound around the posts on the edges of the square hole. On the right is a 60 second exposure of a star at an altitude of about 60 degrees, taken with the astrometric grid placed at a pupil in front of the focal plane mask occulter. The 454 μm occulter is 4.7 resolution elements across at the H-band center wavelength, or 42 mas. The image shown is unreduced HAWAII-2R data. The photometric and astrometric fiducial is the cross pattern of 'ghost' stripes clearly visible at about 2 arcseconds from the central star. It can be rotated to enable the ghosts to be placed at any desired position angle. The Strehl ratio is likely between 85% and 90% (this data is not fully reduced yet).
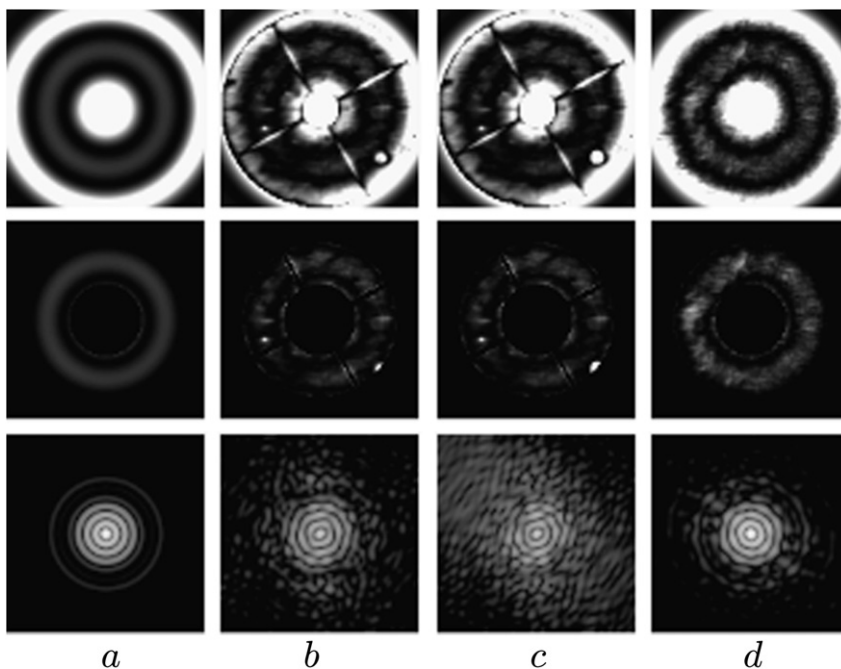

Fig. 5. Simulations showing the effects of the observed I-band pupil illumination non-uniformity combined with simulated phase aberrations from a pinned actuator. The greyscales are not inverted. The top row shows the full Lyot plane intensity, the second row the stopped-down Lyot plane for the L4 stop, after the 445 μm diameter FPM, at the H-band central wavelength. All pupil plane intensities are shown with the same linear greyscale. The bottom row shows the corresponding coronagraphic images on the same logarithmic greyscale. Column a has with no phase or amplitude aberrations in the simulation. Column b includes the quasi-static and static pupil amplitude non-uniformities, but no phase aberrations. Column c includes a 1.25 μm deep dip in the OPD at the location of the largest bright spot in pupil, at about 4 o'clock (the top and middle frames in this column are the same as those in column b). Column d incorporates scintillation determined from video rate pupil camera data. The spiders, not being exactly conjugated to this pupil, flat-field out of the scintillation data in this column (see [13,15,14] for details). The difference between the coronagraphic images in b and c is due to the addition of the pinned actuator's phase error. The measured atmospheric scintillation itself (d) affects the final image's dynamic range about a factor of 50 times less than do failed DM actuator artifacts.

understanding their morphology will be done. Our plan is to leave the grid in place during all exposures in order to align frames to sub-pixel accuracy in the data analysis pipeline.

3. Results

3.1. Pupil illumination

The *I*-band optical CCD camera used to align the Lyot stop was used to examine pupil illumination and scintillation at video rates, with the target star moved off the occulting hole on the FPM (see [13,15] for details of the data acquisition and reduction). We separated out video-rate fast intensity variations in pupil (presumably due to scintillation) from a slow illumination pattern associated with the optics alone. Note that since the spiders are not conjugated to the DM or primary mirror, they flat-field out of the data in the individual CCD frames in our data processing (see [13]).
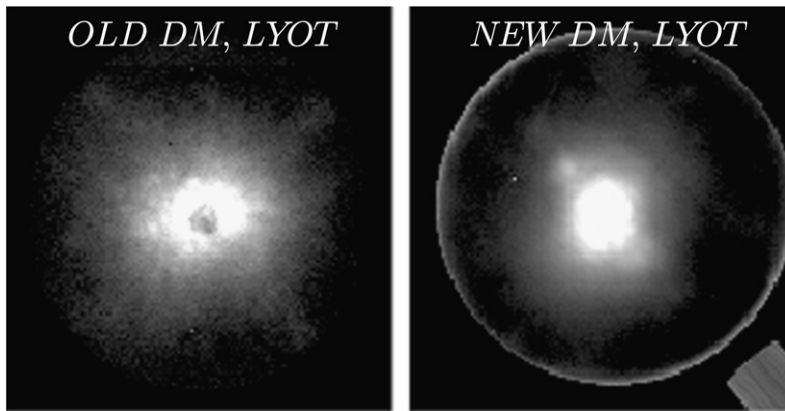

Fig. 6. Left: *H* band coronagraphic PSF with the older DM. Right: Coronagraphic PSF with the replaced, fully-functional DM (right). The circle is a field stop in the Kermit camera. Both *H*-band PSFs are shown on a square root stretch to display speckle structure in the wings, and the same spatial scale. The two stars shown are not the same object. Note the smoother PSF wings in the right hand image.
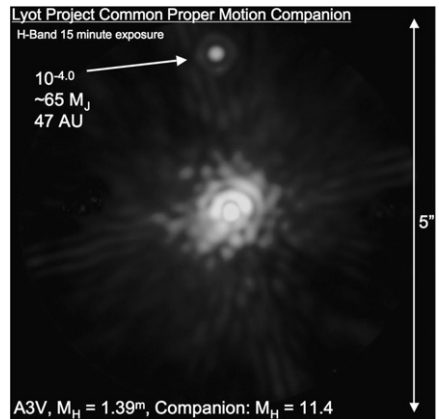
Fig. 7. A faint proper motion companion detected with the old DM, and Lyot stop with thin spider obstructions. This image demonstrates the capabilities of the Lyot Project coronagraph prior to recent improvements.
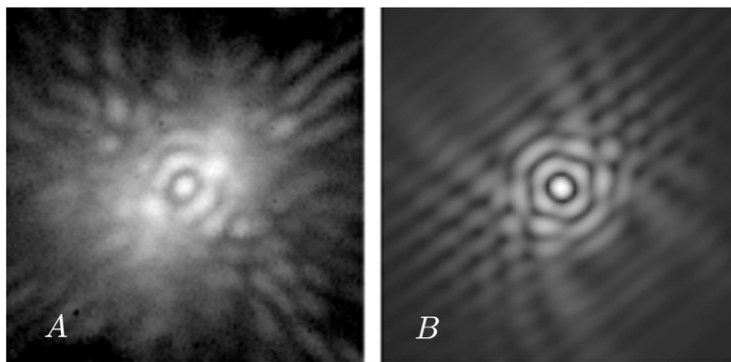

Fig. 8. The *H*-band coronagraphic PSF of Vega from an 8 second exposure taken in May 2005 (A), and a simulated broad band coronagraphic image (B). The exposure time was 8 seconds, the detector pixel scale is 13.5 milliarcseconds. The elongation (approximately diagonal, lower left to upper right) was due to broken actuators on the AO system's DM. The elongation is at an angle of 45° from the top of the image in all cases prior to derotation of the data such that N is up and E is left in the image. The Strehl ratio in this image is approximately 92% (for an unocculted star). Each image is 3.2 arcseconds across. The DM shape used in the Fraunhofer approximation broad band simulation reproduces five pinned actuators that were present in the AEOS DM prior to September 2006. Both frames display a similar rectangular morphology and speckling. In order to match the contrast present in these data, the simulations have a uniform plateau of 1% of the peak coronagraphic intensity arbitrarily added to the image. Without this added floor the simulation has a far higher dynamic range than the data. However, AEOS's secondary mirror support spider vanes were not modelled in (B).
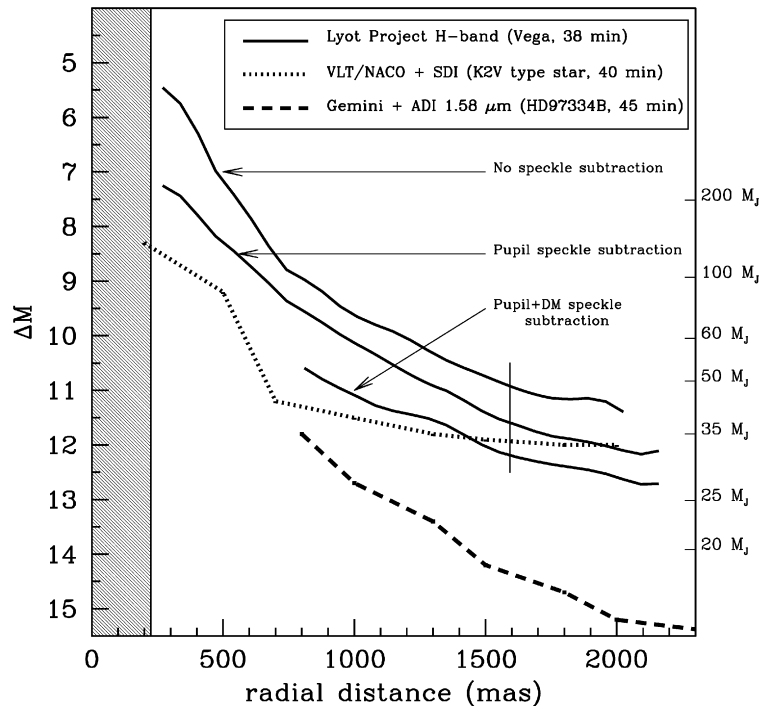
Fig. 9. Dynamic range plots after reducing 284 8-second exposure time images of Vega (after [25]) taken with the old DM. The solid lines depict azimuthally-averaged radial profiles of the *H*-band detection limit incorporating 284 images. These curves show our sensitivity with no speckle subtraction at all, after subtracting the static pupil speckle pattern, and after those speckles due to the imperfections in the DM have further been subtracted (the spiders, DM, and sky all rotate with respect to each other). Our speckle identification follows the Angular Differential Imaging (ADI) technique [26]. The shaded region at left represents the radius of our occulting mask. The dotted line represents the VLT/NACO sensitivities with the Simultaneous Differential Imaging (SDI) analysis technique [27,28]. The dashed line shows Gemini results [26] using the ADI technique on the star HD97334B. The vertical line at 1593 mas shows the extent of the AEOS AO control radius [3]. The corresponding upper limits to companion masses at right are based on models and apply only to the Lyot Project results. The other programs may have different mass limits, given their sensitivities to e.g. methanated companions.

These data are shown in Fig. 5. A feature of the variation in pupil intensity was due to a failed actuator on AEOS's old DM. Using a simple model of a pinned actuator we show simulated coronagraphic PSFs that would result from the observed pupil non-uniformities with and without phase error due to a pinned actuator. We concluded that the failed actuator's phase error had a worse effect than the observed *I*-band pupil illumination non-uniformity when observing at *H*. The actual optics-induced *H*-band illumination non-uniformity is expected to be less than that shown in Fig. 5. The observed *I*-band atmospheric scintillation is not fully sampled at video rates, and thus is underestimated in our measurements. However, scintillation at *H* is expected to be lower than at *I*. While we have no way of estimating the way our *I* measurements scale to *H*, we calculated what the observed scintillation alone would do to a coronagraphic PSF in the figure. This degradation of contrast was also far below that of the failed actuator. This experiment has not been repeated with the new fully-functional AEOS DM installed September 2006, with its noticeably improved PSF (Figs. 6 and 7).

Data and simulated PSFs show similar features (Fig. 8). Speckles caused by a failed actuator resemble some of the long-lived PSF features found by [25] using the old DM with frozen actuators. The full broadband simulation predicts an elongated, boxy PSF. This is what (Fig. 8) shows. Within 1 arcsecond of the primary star, the sensitivity of the Lyot Project Coronagraph is reduced by a factor of up to 50 compared to what it should be achieving on AEOS, unless speckle suppression techniques inspired by [26] are used (see [25] for details, and Fig. 9).

4. Future plans

A *J H* integral field unit spectrograph will replace the Kermit imaging camera by late 2008, and an apodized pupil Lyot coronagraph will be implemented on the Lyot Project in 2007. We expect the dynamic range of the coronagraph

to increase markedly as a result of these upgrades. Our polarization data from the coronagraph is still being reduced, and will be reported on elsewhere in the near future. Astrometric and photometric fiducial ghost methods discussed here promise significant scientific returns enabling photometry and common proper motion to be measured accurately with coronagraphs, in addition to being technical trail blazers in the search for and characterization of extrasolar planets.

Acknowledgements

References

[1] M. Troy, R.G. Dekany, G. Brack, B.R. Oppenheimer, E.E. Bloemhof, T.L. Hayward, T. Trinh, F.G. Dekens, F. Shi, B. Brandl, Palomar adaptive optics project: Status and performance, in: Adaptive Optical Systems Technologies, Proceedings of the SPIE, vol. 4007, 2000, pp. 31–40.

[2] T.L. Hayward, B. Brandl, B. Pirger, C. Blacken, G.E. Gull, J. Schoenwald, J. Houck, PHARO: a near-infrared camera for the Palomar Hale 5 m telescope, Publications of the Astronomical Society of the Pacific 113 (February 2001) 105–118.

[3] A. Sivaramakrishnan, C.D. Koresko, R.B. Makidon, T. Berkefeld, M.J. Kuchner, Ground-based coronagraphy with high-order adaptive optics, Astrophys. J. 552 (May 2001) 397–408.

[4] B.R. Oppenheimer, R.G. Dekany, T.L. Hayward, B. Brandl, M. Troy, E.E. Bloemhof, Companion detection limits with adaptive optics coronagraphy, in: Adaptive Optical Systems Technologies, Proceedings of the SPIE, vol. 4007, 2000, pp. 899–905.

[5] B. Lyot, The study of the solar corona and prominences without eclipses (George Darwin lecture, 1939), Monthly Notices of the Royal Astronomical Society 99 (June 1939) 580.

[6] B.A. Macintosh, B. Bauman, J. Wilhelmsen Evans, J.R. Graham, C. Lockwood, L. Poyneer, D. Dillon, D.T. Gavel, J.J. Green, J.P. Lloyd, R.B. Makidon, S. Olivier, D. Palmer, M.D. Perrin, S. Severson, A.I. Sheinis, A. Sivaramakrishnan, G. Sommargren, R. Soummer, M. Troy, J.K. Wallace, E. Wishnow, Extreme adaptive optics planet imager: overview and status, in: Advancements in Adaptive Optics, Proceedings of the SPIE, vol. 5490, October 2004, 359–369.

[7] J.-L. Beuzit, M. Feldt, D. Mouillet, C. Moutou, K. Dohlen, P. Puget, T. Fusco, P. Baudoz, A. Boccaletti, S. Udry, D. Ségransan, R. Gratton, M. Turatto, H.-M. Schmid, R. Waters, D. Stam, P. Rabou, A.-M. Lagrange, F. Ménard, J.-C. Augereau, M. Langlois, F. Vakili, L. Arnold, T. Henning, D. Rouan, M. Kasper, N. Hubin, A planet finder instrument for the VLT, in: C. Aime, F. Vakili (Eds.), IAU Colloq. 200: Direct Imaging of Exoplanets: Science & Techniques, 2006, pp. 317–322.

[8] J.P. Lloyd, J.R. Graham, P. Kalas, B.R. Oppenheimer, A. Sivaramakrishnan, R.B. Makidon, B.A. Macintosh, C.E. Max, P. Baudoz, J.R. Kuhn, D. Potter, Astronomical coronagraphy with high-order adaptive optics systems, in: A.R. Pirich, P.L. Repak, P.S. Idell, S.R. Czyzak (Eds.), Multifrequency Electronic/Photonic Devices and Systems for Dual-Use Applications, Proceedings of the SPIE, vol. 4490, December 2001, pp. 290–297.

[9] M.D. Perrin, J.R. Graham, M. Trumpis, J.R. Kuhn, K. Whitman, R. Coulter, J.P. Lloyd, L.C. Roberts, First light with the kermit, in: P.W. Kervin, J.L. Africano (Eds.), 2002 AMOS Technical Conference, March 2003.

[10] J.P. Lloyd, A. Sivaramakrishnan, Tip-tilt error in Lyot coronagraphs, Astrophys. J. 621 (March 2005) 1153–1158.

[11] A. Sivaramakrishnan, R. Soummer, A.V. Sivaramakrishnan, J.P. Lloyd, B.R. Oppenheimer, R.B. Makidon, Low-order aberrations in band-limited Lyot coronagraphs, Astrophys. J. 634 (December 2005) 1416–1422.

[12] A. Sivaramakrishnan, J.P. Lloyd, Spiders in Lyot coronagraphs, Astrophys. J. 633 (November 2005) 528–533.

[13] A. Sivaramakrishnan, M.D. Perrin, R.B. Makidon, R. Soummer, B.R. Oppenheimer, A.P. Digby, Performance predictions of second stage adaptive optics coronagraphy on the AEOS telescope, in: P.W. Kervin, J.L. Africano (Eds.), 2003 AMOS Technical Conference, September 2003.

[14] A. Sivaramakrishnan, B.R. Oppenheimer, M.D. Perrin, L.C. Roberts, R.B. Makidon, R. Soummer, A.P. Digby, L.W. Bradford, M.A. Skinner, N.H. Turner, T.A. Ten Brummelaar, Scintillation and pupil illumination in AO coronagraphy, in: C. Aime, F. Vakili (Eds.), IAU Colloq. 200: Direct Imaging of Exoplanets: Science & Techniques, 2006, pp. 613–616.

[15] B.R. Oppenheimer, A. Sivaramakrishnan, M.D. Perrin, R.B. Makidon, R. Soummer, L.C. Roberts, L.W. Bradford, M.A. Skinner, T. Ten Brummelaar, N.H. Turner, Scintillation in high dynamic range coronagraphy, in: P.W. Kervin, J.L. Africano (Eds.), 2005 AMOS Technical Conference, September 2005.

[16] M.D. Perrin, J.R. Graham, P. Kalas, J.P. Lloyd, C.E. Max, D.T. Gavel, D.M. Pennington, E.L. Gates, Laser guide star adaptive optics imaging polarimetry of Herbig Ae/Be stars, Science 303 (February 2004) 1345–1348.

[17] A.P. Digby, S. Hinkley, B.R. Oppenheimer, A. Sivaramakrishnan, J.P. Lloyd, M.D. Perrin, L.C. Roberts Jr., R. Soummer, D. Brenner, R.B. Makidon, M. Shara, J. Kuhn, J. Graham, P. Kalas, L. Newburgh, The challenges of coronagraphic astrometry, Astrophys. J. 650 (October 2006) 484–496.

[18] A. Sivaramakrishnan, B.R. Oppenheimer, Astrometry and photometry with coronagraphs, Astrophys. J. 647 (August 2006) 620–629.

[19] C. Marois, D. Lafrenière, B.A. Macintosh, R. Doyon, Accurate astrometry and photometry of saturated and coronagraphic point spread functions, Astrophys. J. 647 (August 2006) 612–619.

[20] C. Aime, R. Soummer, A. Ferrari, Total coronagraphic extinction of rectangular apertures using linear prolate apodizations, Astron. Astrophys. 389 (2002) 334–344.

[21] R. Soummer, C. Aime, P.E. Falloon, Stellar coronagraphy with prolate apodized circular apertures, Astron. Astrophys. 397 (January 2003) 1161–1172.

[22] R. Soummer, Apodized pupil Lyot coronagraphs for arbitrary telescope apertures, Astrophys. J. 618 (January 2005) L161–L164.

[23] B.R. Oppenheimer, A.P. Digby, L. Newburgh, D. Brenner, M. Shara, J. Mey, C. Mandeville, R.B. Makidon, A. Sivaramakrishnan, R. Soummer, J.R. Graham, P. Kalas, M.D. Perrin, L.C. Roberts, J.R. Kuhn, K. Whitman, J.P. Lloyd, The Lyot project: toward exoplanet imaging and spectroscopy, in: D. Bonaccini Calia, B.L. Ellerbroek, R. Ragazzoni (Eds.), Advancements in Adaptive Optics, Proceedings of the SPIE, vol. 5490, October 2004, pp. 433–442.

[24] L.W. Bradford, L.C. Roberts, M.A. Skinner, A.P. Digby, B.R. Oppenheimer, M.D. Perrin, N.H. Turner, Observations of scintillation with AEOS, in: P.W. Kervin, J.L. Africano (Eds.), 2005 AMOS Technical Conference, September 2005.

[25] S. Hinkley, B.R. Oppenheimer, R. Soummer, A. Sivaramakrishnan, L.C. Roberts Jr., J. Kuhn, R.B. Makidon, M.D. Perrin, J.P. Lloyd, K. Kratter, D. Brenner, Temporal evolution of coronagraphic dynamic range and constraints on companions to Vega, Astrophys. J. 654 (January 2007) 633–640.

[26] C. Marois, D. Lafrenière, R. Doyon, B.A. Macintosh, D. Nadeau, Angular differential imaging: A powerful high contrast technique, Astrophys. J. 641 (April 2006) 556–564.

[27] B.A. Biller, L.M. Close, E. Masciadri, R. Lenzen, W. Brandner, D. McCarthy, T. Henning, E.L. Nielsen, M. Hartung, S. Kellner, K. Geissler, M. Kasper, Contrast limits with the Simultaneous Differential Extrasolar Planet Imager (SDI) at the VLT and MMT, in: B.L. Ellerbroek, C.D. Bonaccini (Eds.), Advances in Adaptive Optics II, Proceedings of the SPIE, vol. 6272, July 2006, pp. 62722D.

[28] M. Kasper, N. Ageorges, A. Boccaletti, W. Brandner, L.M. Close, R. Davies, G. Finger, R. Genzel, M. Hartung, A. Kaufer, S. Kellner, N. Hubin, R. Lenzen, C. Ludman, G. Monnet, A. Moorwood, T. Ott, P. Riaud, H.-J. Roser, D. Rouan, J. Spyromilio, New observing modes of NACO, The Messenger 119 (March 2005) 11.